Journal for ImmunoTherapy of Cancer

Attention-guided framework for integrative omics and temporal dynamics in predicting major pathological response in neoadjuvant immunochemotherapy for NSCLC

Xiangfeng Gan,[1] Jianzhong He,[2] Wei Zhang,[3] Wenzeng Chen,[4] Shijiancong Liu,[1] Wenhao Li,[5] Xiaohui Duan,[6] Liangzhan Lv,[1] Yi Liang,[5] Qingdong Cao,[1] Baishen Chen [3]

To cite: Gan X, He J, Zhang W, *et al*. Attention-guided framework for integrative omics and temporal dynamics in predicting major pathological response in neoadjuvant immunochemotherapy for NSCLC. *Journal for ImmunoTherapy of Cancer* 2025;**13**:e012526. doi:10.1136/jitc-2025-012526

► Additional supplemental material is published online only. To view, please visit the journal online (https://doi.org/10.1136/jitc-2025-012526).

XG, JH and WZ contributed equally.

Accepted 04 October 2025

For numbered affiliations see end of article.

Correspondence to
Dr Baishen Chen;
ganxf@mail3.sysu.edu.cn

Qingdong Cao;
caoqd@mail.sysu.edu.cn

Yi Liang;
yiliangzscph@outlook.com

ABSTRACT

Objective This study developed a multiomics model combining radiomics, pathomics, and temporal imaging to predict major pathological response in patients with locally advanced non-small cell lung cancer (NSCLC) undergoing neoadjuvant immunochemotherapy.

Methods A retrospective, multicenter study was conducted, enrolling 271 patients with stage IB–III NSCLC who received neoadjuvant immunochemotherapy. High-resolution CT images were enhanced using a generative adversarial network-based super-resolution technique. Radiomics features were extracted from multi-sequence CT scans at multiple time points, while pathomics features were derived from whole-slide imaging of surgical specimens. A transformer-based attention mechanism was used to integrate radiomics, pathomics, and temporal imaging data. The model was trained and validated on data from one center and tested on external cohorts. Performance was evaluated using area under the curve (AUC), net reclassification improvement, integrated discrimination improvement, and decision curve analysis.

Results The Trans-Model demonstrated superior predictive performance, achieving an AUC of 0.858 (95% CI 0.783 to 0.933) in the external test cohort. It outperformed Rad-Model (AUC: 0.839) and Patho-Model (AUC: 0.753). The Trans-Model effectively stratified patients by survival outcomes, with major pathological response (MPR)-positive patients exhibiting significantly improved 3-year overall survival (87.3% vs 76.1%, p=0.034) and 5-year progression-free survival (45.8% vs 34.7%, p=0.033) compared with MPR-negative patients. Decision curve analysis confirmed the model's clinical utility across a wide range of threshold probabilities.

Conclusion The multiomics model, integrating multi-temporal, multi-sequence data with attention-based feature fusion, improves MPR prediction in patients with NSCLC receiving neoadjuvant immunochemotherapy, enabling personalized treatment by identifying responders and optimizing outcomes.

WHAT IS ALREADY KNOWN ON THIS TOPIC

⇒ Neoadjuvant immunochemotherapy enhances pathological responses in locally advanced non-small cell lung cancer, but variable major pathological response (MPR) rates and limited biomarkers like Programmed Cell Death-Ligand 1 necessitate better predictive tools. Most artificial intelligence models rely on single-time point imaging, missing treatment-induced changes.

WHAT THIS STUDY ADDS

⇒ A transformer-based Trans-Model integrating multi-temporal radiomics, pathomics, and deep learning achieves an area under the curve of 0.858, outperforming single-modality models and improving survival stratification for MPR-positive patients.

HOW THIS STUDY MIGHT AFFECT RESEARCH, PRACTICE OR POLICY

⇒ This model advances multiomics integration, guiding future oncology research and supporting personalized treatment by identifying responders, potentially influencing cancer care guidelines.

INTRODUCTION

Advanced non-small cell lung cancer (NSCLC) continues to exhibit a poor prognosis; however, surgical intervention has been shown to significantly enhance long-term survival in patients whose tumors have been downstaged by neoadjuvant therapy.[1 2] Neoadjuvant chemotherapy yields pathological complete response (pCR) rates of only 2%– 5.7% and major pathological response (MPR) rates of 12%–15%.[3–6] Recent phase III trials indicate that neoadjuvant immunochemotherapy effectively reduces the risk of postoperative recurrence while also improving rates of pCR and MPR in patients with locally advanced resectable NSCLC.[3–11]

Despite the promising outcomes of neoadjuvant immunochemotherapy, not all patients benefit. Challenges such as immune-related adverse events, potential surgical delays, increased disease progression risk, and complexities of subsequent surgeries complicate clinical management.[12–14] Therefore, identifying predictive biomarkers for MPR in locally advanced NSCLC is crucial to optimizing treatment strategies and minimizing risks, especially given the significant number of patients who do not achieve MPR.

Current biomarker-based approaches to identify patients likely to benefit from neoadjuvant immunotherapy remain limited by a lack of robust evidence. Studies suggest that high Programmed Cell Death-Ligand 1 (PD-L1) expression on tumor cells and programmed cell death protein-1-expressing tumor-infiltrating lymphocytes in the tumor microenvironment are favorable prognostic indicators.[4 15–17] While the greatest therapeutic benefits have been observed in patients exhibiting high levels of PD-L1, improvements in pathological response rates have been documented across all enrolled cohorts, irrespective of PD-L1 expression status. These findings suggest that PD-L1 expression alone is insufficient to robustly stratify patients with superior responses to immunotherapy. The NADIM study highlighted limitations of conventional imaging, showing that pseudolesions from lymphocyte infiltration led to pCR in 33% of patients with radiologically stable disease and 73% with partial response, indicating challenges in standard radiologic evaluation.[18] Recent advances have applied artificial intelligence to medical imaging for predicting pathological response, but most studies rely on single pretreatment imaging time points.[19–21] Effective assessment requires analysis of multisequence, longitudinal imaging changes before and after neoadjuvant therapy. Additionally, integration of multiomics data, such as pathomics, remains underexplored despite its potential to enhance predictive accuracy. To address these gaps, this study used a generative adversarial network (GAN)-based image enhancement technique and a transformer-based feature fusion method developed previously. Radiomics and deep learning (DL) models were built using high-resolution CT images across multiple sequences and time points. By incorporating pathomics features, a multiomics model was established to predict MPR. This approach may improve clinical decision-making and support personalized treatment for patients with resectable NSCLC.

METHODS

Study design and population

This retrospective study included patients with pathologically confirmed NSCLC, clinically staged IB–III, who underwent at least two cycles of neoadjuvant immunochemotherapy. Baseline testing confirmed no tumor driver mutations eligible for first-line targeted therapy. Consecutive cases from April 2018 (Center 1 and 2) and March 2019 (Centers 3) to December 2024 were included (figure 1). After screening, 118 patients from Center 1, 89 from Center 2, and 64 from Center 3 were enrolled. The dataset from Center 1 was partitioned into training and validation sets in a 7:3 ratio, while datasets from Centers 2 and 3 were combined and used as the test cohort. Follow-up details are available in online supplemental file 1.

Pretreatment evaluation

Prior to the initiation of neoadjuvant therapy, patients underwent a thorough evaluation that included contrast-enhanced MRI of the head, contrast-enhanced CT of the chest, abdominal ultrasound, and whole-body bone scintigraphy or Positron Emission Tomography/Computed Tomography (PET-CT). Additionally, bronchoscopy or endobronchial ultrasound-guided bronchoscopy was conducted to obtain biopsy specimens, primarily through endoscopic techniques or CT-guided percutaneous lung puncture. The neoadjuvant immunochemotherapy regimen comprised two to three cycles administered at 3-week intervals, using first-line immune checkpoint inhibitors such as pembrolizumab (200 mg), nivolumab (360 mg), tislelizumab (200 mg), or camrelizumab (200 mg) in conjunction with platinum-based chemotherapy, as per established clinical guidelines. Surgical resection, along with systematic lymph node dissection, was performed 4–6 weeks following the completion of therapy. Baseline CT scans were obtained within 7 days before treatment initiation, while preoperative CT scans were systematically performed within 7 days prior to surgical resection to ensure temporal consistency. The specific treatment regimens, number of therapy cycles, and surgical timelines were collaboratively determined through

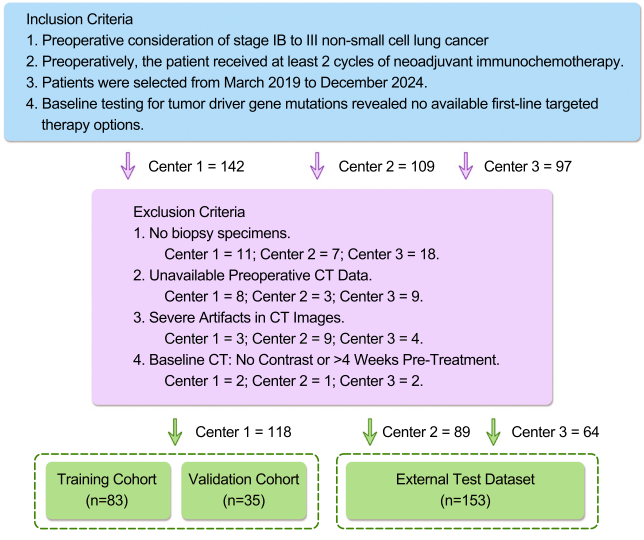

Figure 1 Flow diagram of the study population.

discussions within a multidisciplinary team, ensuring a tailored approach to each patient's care.

Image preprocessing and super-resolution image reconstruction based on GAN

To achieve consistent spatial resolution, all CT scans were resampled to standardized voxel dimensions of 1×1×1 mm, and imaging parameters were adjusted to conform to lung and mediastinal window settings (online supplemental file 2). A super-resolution image reconstruction method, leveraging a GAN designed based on prior advancements, was applied in this study. This technique enabled the enhancement of spatial resolution from the initial voxel size of 1×1×1 mm to an improved resolution of 0.25×0.25×1 mm. For DL applications, the largest cross-sectional slice in the axial plane was selected and extracted as the input dataset. The CT feature extraction and DL training process are detailed in online supplemental file 3.

Model ensemble

In this study, we developed a unified feature fusion framework based on a transformer architecture to integrate high-dimensional, multi-source data (figure 2). A critical preprocessing step was performed prior to fusion to create a standardized, low-dimensional input space and mitigate the risk of overfitting. Specifically, we applied principal component analysis to each feature set—radiomics, DL, and pathomics—reducing their dimensionality to 32 principal components, which collectively explained over 95% of the variance in the original data. This transformer-based framework was systematically applied to construct our predictive models. For multimodal integration, the Tempo-Model was built by fusing the 32-component representations of radiomics and DL features. The final Trans-Model extended this by integrating the 32-component representations from all three sources: radiomics, DL, and pathomics. The core of the fusion mechanism leverages the transformer's attention capabilities. Self-attention mechanisms were used to capture intramodal dependencies by dynamically re-weighting features within each source.[22–24] Concurrently, cross-attention mechanisms were employed to model intermodal relationships, enabling effective information exchange and integration by processing queries, keys, and values from distinct feature sets.[23]

Following the attention mechanisms, layer normalization was applied to stabilize learning and ensure smooth gradient flow.[22] A position-wise feed-forward network was used to refine features, while residual connections and dropout were introduced to enhance robustness and prevent overfitting. The enriched feature representations were concatenated into a unified vector and fed into fully connected layers for classification.[23 24]

Pathological evaluation

Pathological response was assessed based on the percentages of viable tumor cells, necrosis, and stroma within the primary tumor bed.[25] MPR was defined as ≤10% viable tumor cells. Specimens were independently evaluated by experienced pathologists from the JH team, each with over 10 years of experience, with discrepancies resolved through consensus. Details on whole slide image (WSI) data processing and weakly supervised learning are provided in online supplemental file 4.

Pathomics feature aggregation

Two multiple instance learning methods, the histogram method and bag of words (BoW), were developed to aggregate prediction probabilities of pathology patches. In the histogram method, patch prediction probabilities from WSIs were binned into fixed intervals, and patch frequencies were calculated to generate L2-normalized histogram feature vectors representing spatial distributions. In the BoW method, k-means clustering was applied to construct a dictionary of N visual words from training set patch predictions. Each patch was assigned to its nearest visual word, and term frequency (TF) and inverse document frequency (IDF) were combined to produce TF-IDF feature vectors. Features from both methods were normalized and fused through feature concatenation, yielding joint feature representations for downstream pathological analysis (figure 2).

Statistical analysis and model evaluation

All statistical analyses were conducted using SPSS (V.26.0) and Python (V.3.7). Continuous variables were tested with the z-test for normal distributions or the Wilcoxon test for non-normal distributions, while categorical variables were analyzed using the χ^2 test or Fisher's exact test. Multivariable logistic regression with forward stepwise selection identified independent predictors, and survival differences were assessed using Kaplan-Meier curves with the log-rank test. Statistical significance was set at $p<0.05$. Predictive models were evaluated using metrics like Receiver Operating Characteristic (ROC) curves (area under the curve (AUC) compared via DeLong test), net reclassification improvement (NRI), integrated discrimination improvement (IDI), decision curve analysis (DCA), and calibration curves to assess model performance, clinical utility, and agreement with observed outcomes.

RESULTS

Patient characteristics

In accordance with the predefined inclusion and exclusion criteria (figure 1), a total of 271 patients were enrolled in the study. Center 1 contributed 118 patients, of whom 83 were assigned to the training cohort and 35 to the validation cohort. Center 2 included 89 patients, and Center 3 enrolled 64 patients, both serving as the test dataset. Detailed baseline characteristics are summarized in table 1 and online supplemental table S1 and figure S1. Statistical analysis revealed significant differences in Ki-67 expression, lymphovascular invasion status, and STAT status among the cohorts. Univariate and

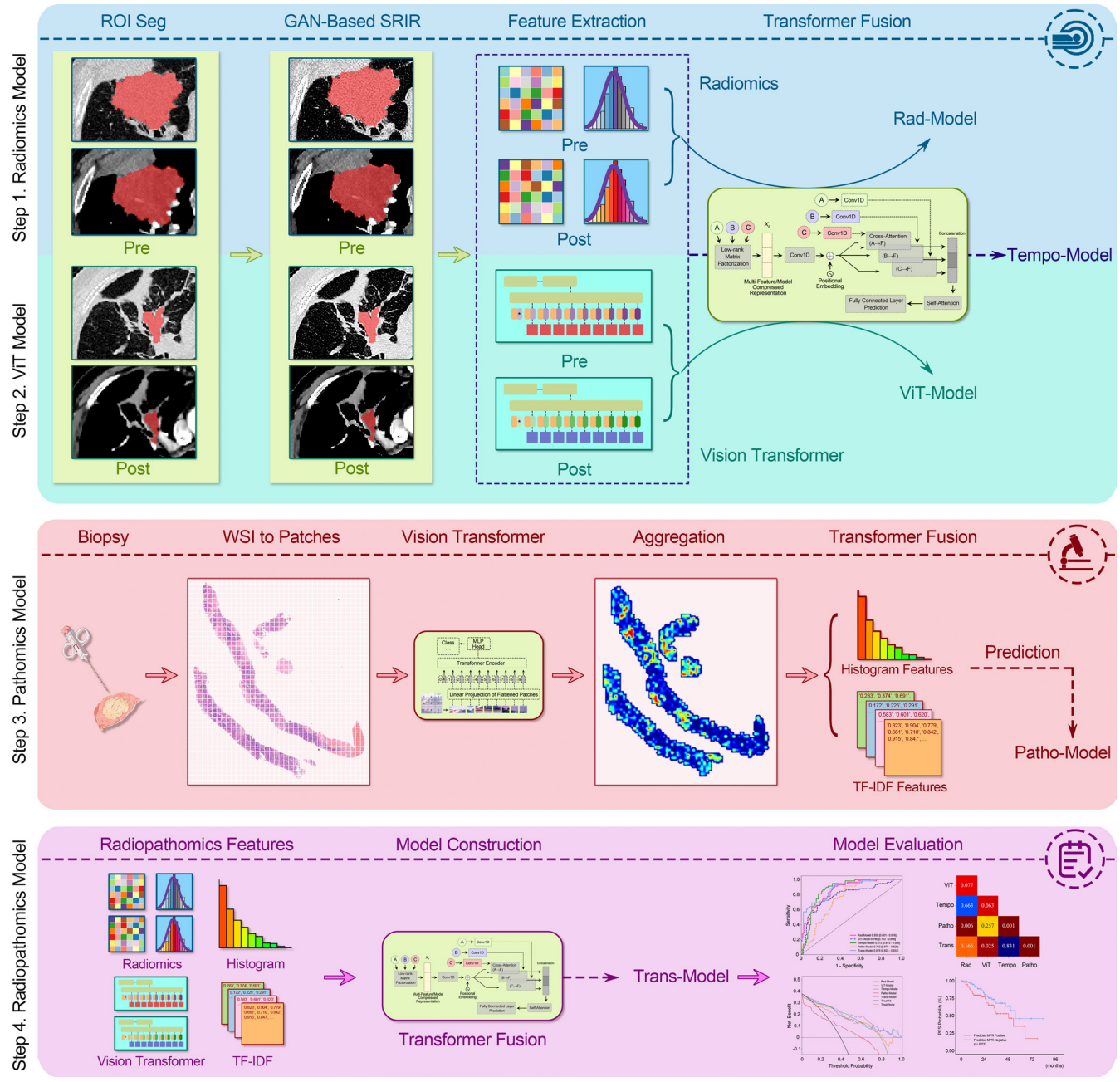

Figure 2 The workflow of the study. The study workflow comprises initial data preprocessing followed by four main modeling steps. Preprocessing: contrast-enhanced CT scans (lung and mediastinal windows) were acquired at two time points (pre-neoadjuvant and post-neoadjuvant therapy), creating four image sequences. Tumor ROIs were delineated, and images were enhanced using a GAN-based super-resolution algorithm to 0.25×0.25×1 mm³ resolution. Step 1: Rad-Model Construction. 1834 radiomic features were extracted from each of the four CT sequences and fused using a transformer-based method to build the Rad-Model. Step 2: ViT-Model and Tempo-Model Construction. A deep learning model extracted 2048 features from each CT sequence. These features were similarly fused using the transformer framework to build the ViT-Model. Step 3: Patho-Model Construction. WSIs were partitioned into 512×512 pixel patches. Patch-level predictions from WSIs were generated using a vision transformer and aggregated via multiple instance learning into 206 pathomics features, which were then used to build the Patho-Model. Step 4: Trans-Model Construction. To build the multimodal Tempo-Model, radiomic and DL feature sets were each reduced to 32 components via PCA and then integrated using the transformer. To build the final multiomics Trans-Model, radiomic, DL, and pathomics feature sets were all independently reduced to 32 components via PCA and subsequently fused using the same transformer-based framework. DL, deep learning; GAN, generative adversarial network; IDF, inverse document frequency; PCA, principal component analysis; ROIs, regions of interest; SRIR, super-resolution image reconstruction; TF, term frequency; WSIs, whole slide images.

Table 1 Patient's characteristics across different cohorts

	All cohorts	Training cohort	Validation cohort	External test cohort	P value
Age	61.38±9.068	60.47±10.037	63.60±7.897	61.37±8.728	0.231
Sex					0.228
Male	222 (81.9)	63 (23.2)	30 (11.1)	129 (48.6)	
Female	49 (18.1)	20 (7.4)	5 (1.8)	24 (8.9)	
Smoking history					0.766
Negative	133 (49.1)	38 (14.0)	18 (6.6)	77 (28.4)	
Positive	138 (50.9)	45 (16.6)	17 (6.3)	76 (28.0)	
Tumor location					0.284
RUL	67 (24.7)	14 (5.2)	6 (2.2)	47 (17.3)	
RML	14 (5.2)	6 (2.2)	2 (0.7)	6 (2.2)	
RLL	67 (24.7)	26 (9.6)	8 (3.0)	33 (12.2)	
LUL	77 (28.4)	22 (8.1)	11 (4.1)	44 (16.2)	
LLL	46 (17.0)	15 (5.5)	8 (3.0)	23 (8.5)	
BMI	23.04±2.493	22.64±1.598	22.84±1.537	23.31±3.010	0.129
SCC	2.82±6.765	3.48±8.445	2.337±3.805	2.57±6.352	0.561
Cyfra211	7.66±9.996	6.98±8.321	9.19±12.850	7.67±10.120	0.549
CEA	6.92±12.051	6.27±6.140	9.32±19.476	6.72±12.297	0.434
Ki-67	0.39±0.281	0.34±0.277	0.33±0.300	0.43±0.272	0.017
Classification of pathological types					0.522
Squamous carcinoma	143 (52.8)	40 (14.8)	20 (22.1)	83 (30.6)	
Adenocarcinoma	104 (38.4)	32 (11.8)	13 (4.8)	59 (21.8)	
Others	24 (8.9)	11 (4.1)	2 (0.7)	11 (4.1)	
MPR					0.061
Negative	150 (55.4)	38 (14.0)	18 (6.6)	94 (34.7)	
Positive	121 (44.6)	45 (16.6)	17 (6.3)	59 (21.8)	
Visceral pleural invasion					0.116
Negative	233 (86.0)	69 (25.5)	34 (12.5)	130 (48.0)	
Positive	38 (14.0)	14 (5.2)	1 (0.4)	23 (8.5)	
Lymphovascular invasion					<0.001
Negative	193 (71.2)	42 (15.5)	34 (12.5)	117 (43.2)	
Positive	78 (28.8)	41 (15.1)	1 (0.4)	36 (13.3)	
STAS					<0.001
Negative	216 (79.7)	55 (20.3)	33 (12.2)	128 (47.2)	
Positive	55 (20.3)	28 (10.3)	2 (0.7)	25 (9.2)	
Differentiation					0.115
Well	132 (48.7)	40 (14.8)	21 (7.7)	71 (26.2)	
Moderately	114 (42.1)	40 (14.8)	10 (3.7)	64 (23.6)	
Poorly	25 (9.2)	3 (1.1)	4 (1.5)	18 (6.6)	
cT stage					0.051
T1	26 (9.6)	7 (2.6)	2 (0.7)	17 (6.3)	
T2	115 (42.4)	35 (12.9)	10 (3.7)	70 (25.8)	
T3	68 (25.1)	15 (5.5)	41 (15.1)	41 (15.1)	
T4	62 (22.9)	26 (9.6)	25 (9.2)	25 (9.2)	
cN stage					0.340
N0	29 (10.7)	10 (3.7)	2 (0.7)	17 (6.3)	
N1	67 (24.7)	20 (7.4)	5 (1.8)	42 (15.5)	
N2	175 (64.6)	53 (19.6)	28 (10.3)	94 (34.7)	

Continued

Table 1 Continued

	All cohorts	Training cohort	Validation cohort	External test cohort	P value
Clinical stage					0.435
II	55 (20.3)	15 (5.5)	5 (1.8)	35 (12.9)	
III	216 (79.7)	68 (25.1)	30 (11.1)	118 (43.5)	

Values are mean±SD or n (%) unless otherwise defined.
BMI, body mass index; CEA, carcinoembryonic antigen; LLL, left lower lobe; LN, lymph node; LUL, left upper lobe; MPR, major pathological response; RLL, right lower lobe; RML, right middle lobe; RUL, right upper lobe; SCC, squamous cell carcinoma antigen; STAS, spread through air spaces.

multivariate analyses revealed that none of these three clinical features were significantly associated with MPR, whereas only smoking history exhibited a statistically significant correlation with MPR (online supplemental table S2).

Kaplan-Meier survival analyses were conducted to evaluate overall survival (OS) and progression-free survival (PFS) across the three cohorts and centers, as presented in online supplemental figure S1. The median follow-up durations were 24 months for Center 1, 28 months for Center 2, and 24 months for Center 3. The 3-year OS rates were estimated at 83.5% (95% CI 71.19% to 90.87%) for Center 1, 86.9% (95% CI 72.61% to 92.79%) for Center 2, and 84.8% (95% CI 71.19% to 90.87%) for Center 3. The 5-year OS rates remain inconclusive due to insufficient follow-up time. The 5-year PFS rates were calculated as 34.6% (95% CI 6.62% to 65.97%) for Center 1, 41.1% (95% CI 11.62% to 71.28%) for Center 2, and 30.9% (95% CI 1.24% to 60.63%) for Center 3.

Performance of models for predicting MPR

In the test cohort, the Trans-Model achieved the highest AUC of 0.858 (95% CI 0.783 to 0.933) (table 2). DCA demonstrated that both the Rad-Model and Trans-Model provided substantial net benefit across a wide range of threshold probabilities (figure 3A). However, the Patho-Model yielded a comparatively lower AUC of 0.753 (95% CI 0.678 to 0.829). Baseline comparisons among cohorts (table 1) revealed higher Ki-67 expression in the test cohort, suggesting increased proliferative activity, while higher rates of lymphovascular invasion and STAT positivity were observed in the training cohort, indicating potentially greater tumor invasiveness. Such intercohort imbalances may partly account for the limited generalizability of the Patho-Model. The results for training and validation cohorts are presented in table 2 and online supplemental figure S2.

Although no statistically significant difference was observed, a higher proportion of patients with cT1-2 stage was noted in the test cohort (table 1). This discrepancy

Table 2 Performance metrics of the models in three cohorts

Model	Cohorts	AUC (95% CI)	Accuracy	Sensitivity	Specificity	PPV	NPV
Rad	Training	0.916 (0.855 to 0.977)	0.843	0.968	0.769	0.714	0.976
	Validation	0.906 (0.791 to 0.998)	0.857	0.923	0.818	0.750	0.947
	Test	0.839 (0.761 to 0.916)	0.757	0.897	0.670	0.627	0.913
ViT	Training	0.902 (0.839 to 0.965)	0.843	0.774	0.885	0.800	0.868
	Validation	0.892 (0.769 to 0.992)	0.829	0.769	0.864	0.769	0.864
	Test	0.790 (0.712 to 0.868)	0.757	0.707	0.787	0.672	0.813
Tempo	Training	0.959 (0.916 to 0.999)	0.880	0.968	0.827	0.769	0.977
	Validation	0.934 (0.843 to 0.998)	0.886	0.692	0.942	0.847	0.846
	Test	0.852 (0.775 to 0.928)	0.803	0.879	0.755	0.689	0.910
Patho	Training	0.844 (0.758 to 0.931)	0.807	0.677	0.885	0.778	0.821
	Validation	0.825 (0.660 to 0.990)	0.800	0.692	0.864	0.750	0.826
	Test	0.753 (0.678 to 0.829)	0.684	0.879	0.564	0.554	0.883
Trans	Training	0.946 (0.901 to 0.991)	0.867	0.903	0.846	0.778	0.936
	Validation	0.923 (0.835 to 0.997)	0.829	0.769	0.864	0.769	0.864
	Test	0.858 (0.783 to 0.933)	0.770	0.897	0.691	0.642	0.915

AUC, area under the curve; NPV, negative predictive value; PPV, positive predictive value.

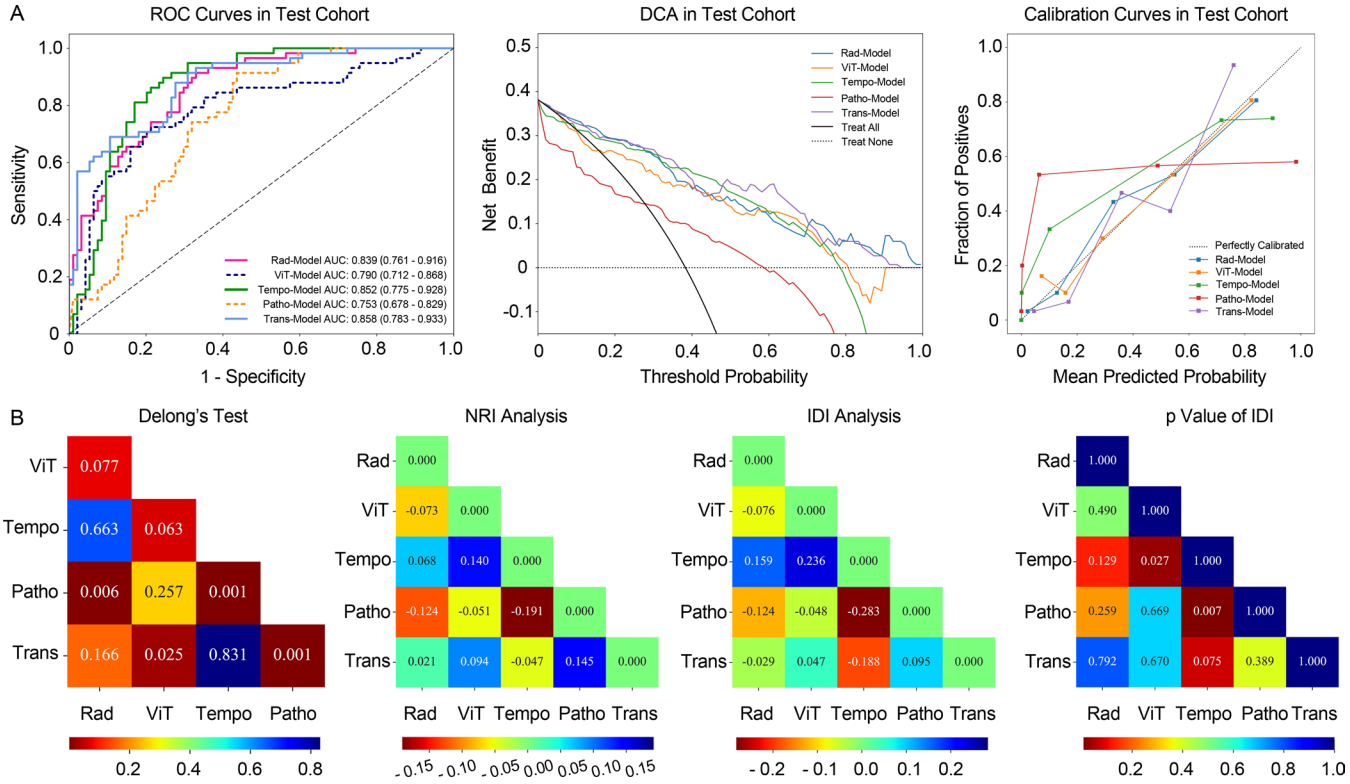

Figure 3 Predictive performance evaluation of each model in the test cohort. (A) ROC, DCA, and calibration curves were analyzed across five models. The Tempo-Model, based on multi-temporal and multimodal CT images, achieved an AUC of 0.852, while the Patho-Model showed lower performance with an AUC of 0.753. The Trans-Model attained the highest AUC of 0.858. (B) Statistical comparisons using DeLong's test indicated that the Trans-Model's AUC improvement over the ViT-Models and Patho-Models was significant. NRI and IDI analyses revealed mixed results: positive and negative NRI values versus Rad-Models and Tempo-Models, respectively, with negative IDI values in both cases. Calibration curves showed no samples in the high-risk region for the Trans-Model, indicating limitations despite its high AUC. The model was more accurate in low-risk and medium-risk predictions but less effective in the high-risk group, likely explaining the NRI and IDI discrepancies. AUC, area under the curve; DCA, decision curve analysis; IDI, integrated discrimination improvement; NRI, net reclassification improvement; ROC, Receiver Operating Characteristic.

may partially explain the inferior performance of the ViT-Model compared with the Rad-Model. The inclusion of radiomic features less influenced by tumor volume, such as texture and gray-level metrics, likely compensated for model performance degradation caused by differences in cT stage, enabling the Rad-Model to achieve an AUC of 0.839 (95% CI 0.761 to 0.916). The intercohort variation in cT stage may have also contributed to reduced predictive accuracy for specific samples during model training. Calibration curves further demonstrated that CT image-based models (Rad-Models, ViT-Models, and Tempo-Models) exhibited poorer predictive performance and lower coverage in the high-risk range (figure 3A). Nevertheless, overall, the Trans-Model, which integrates multi-sequence longitudinal CT data and multiomics features, demonstrated superior predictive performance for MPR and greater clinical utility compared with other models, as shown by DCA (figure 3A).

The Trans-Model demonstrated statistically significant advantages over multiple comparative models as evidenced by DeLong's test (figure 3B), yet certain limitations were identified. In comparison with the Rad-Model, the NRI for Trans versus Rad was 0.021, while the IDI was −0.029. This suggests that, although classification accuracy was enhanced, an overall decline in discriminative ability was observed. This discrepancy can be attributed to the Trans-Model's relatively weaker predictive performance in the high-risk region, which was offset by superior accuracy in low-risk to moderate-risk regions compared with the Rad-Model, thereby raising the overall NRI. However, as IDI is more sensitive to discrimination in high-risk samples, the diminished performance in this critical range led to a negative IDI value.

A similar trend was noted when comparing the Trans-Model with the Tempo-Model. Given the close similarity in AUC values between these models, the Trans-Model's advantage in low-risk and moderate-risk strata proved insufficient to compensate for its reduced effectiveness in the high-risk region. As a result, the NRI and IDI for Trans versus Tempo were −0.047 and −0.188, respectively, with the larger decrease in IDI reflecting its greater sensitivity to high-risk classification. Parallel considerations apply to the comparisons involving the Patho-Model, where $IDI_{Trans\ vs\ Patho}$ was 0.095 (p=0.389) and $IDI_{Tempo\ vs\ Patho}$ was 0.283 (p=0.007), indicating differences in discriminative performance consistent with variations in risk stratification

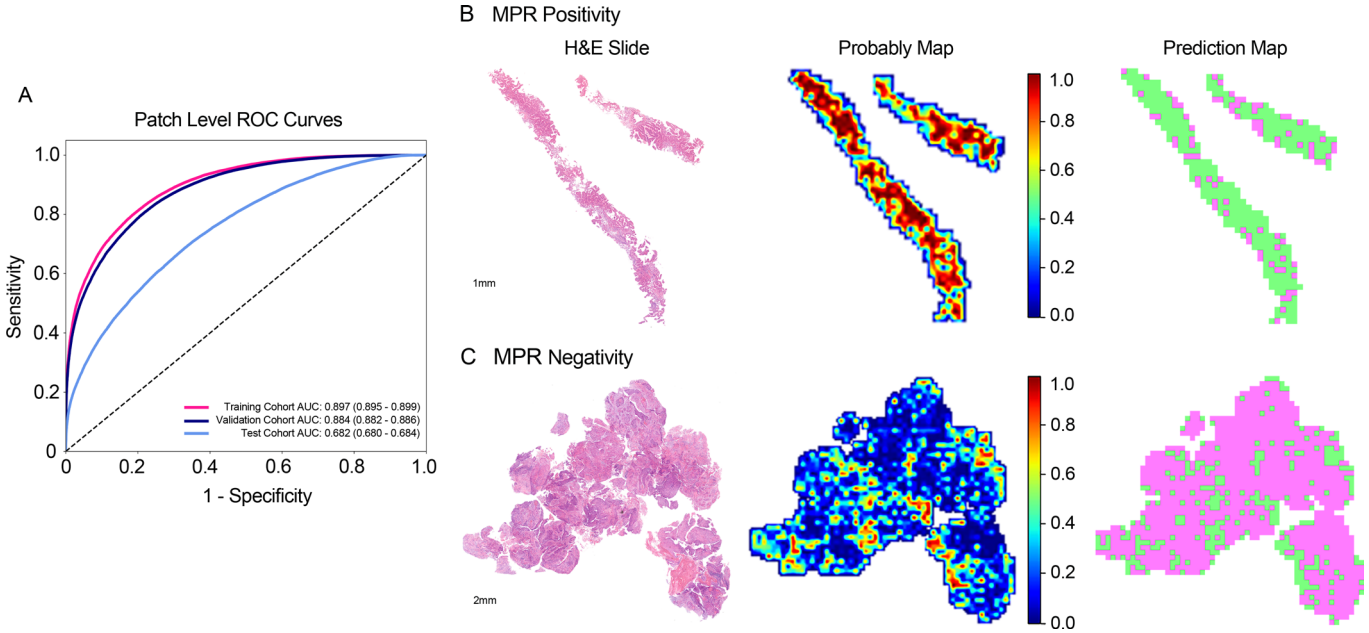

Figure 4 Pathomics model performance evaluation. (A) Patch-level ROC for MPR prediction by the Patho-Model. (B) and (C) Show the H&E whole slide image (left), patch-wise probability heatmap (center), and WSI-level prediction map (right). (B) MPR-positive prediction; (C) MPR-negative prediction by the Patho-Model. AUC, area under the curve; MPR, major pathological response; ROC, Receiver Operating Characteristic; WSI, whole slide image.

capacity. Therefore, this study is primarily intended to support treatment decision-making for patients at low to moderate risk, rather than to replace existing high-risk assessment methods.

The patch-level ROC curve is presented in figure 4A, with an AUC of 0.682 (95% CI 0.680 to 0.684) observed in the test cohort. Two representative cases, in which MPR positivity and negativity were predicted by the Patho-Model, respectively, are illustrated in figure 4B,C. The probability maps and prediction heatmaps produced by the model clearly demonstrate the Patho-Model's high accuracy in evaluating region-specific tiles, highlighting its potential utility for localized pathological assessment.

Survival analysis

The 3-year OS was reported to be 85.3% (95% CI 72.02% to 92.54%) for the training cohort, 82.5% (95% CI 44.90% to 95.48%) for the validation cohort, and 86.1% (95% CI 72.91% to 98.43%) for the test cohort. The 5-year PFS was found to be 0% for the training cohort, 66.5% (95% CI 33.12% to 86.03%) for the validation cohort, and 37.1% (95% CI 23.18% to 51.96%) for the test cohort. As demonstrated in figure 5, the number of patients predicted as MPR positive and negative by the Trans-Model in the external test cohort were 71 and 82, respectively. In the Tempo-Model, these figures were 62 and 91. In the Trans-Model, which integrated pathomics, the 3-year OS for the MPR positive group was reported as 87.3%, while the OS for the negative group was 76.1%. The 5-year PFS for the MPR positive group was 45.8%, compared with 34.7% for the negative group. The p values for the differences between the two groups were found to be 0.034 and 0.033, respectively (figure 5A,B). This finding aligns with the established association between MPR status and improved survival outcomes, indicating that the OS and PFS for the MPR positive group were superior to those of the MPR negative group. These results suggest that even in the absence of confirmed MPR status, the predictions made by the Trans-Model can effectively distinguish patients with different survival trajectories. However, in the Tempo-Model, this discriminative ability was found to be diminished, with p values for OS and PFS reported as 0.024 and 0.428, respectively (figure 5C,D). This indicates that while the Patho-Model may not demonstrate the same predictive efficacy for MPR status as imaging-based models, the information contained within pathomics contributes to the performance of the Trans-Model in stratifying patients based on PFS.

DISCUSSION

NSCLC exhibits a relatively high proportion of MPR following neoadjuvant immunochemotherapy, estimated to be around 33.3%–82.9%, while the proportion of pCR is lower, ranging from approximately 17.2%–63.4%.[4 5 10 17 18 26–29] The distinction between MPR and pCR lies in the fact that MPR not only emphasizes complete remission but also quantifies the extent of residual tumor burden, thereby providing a more accurate reflection of treatment efficacy on tumor load. The NADIM study has demonstrated that the degree of residual tumor cells serves as a critical prognostic factor, with MPR significantly associated with improvements in PFS (88.4% vs 57.1%, p=0.01).[18] Furthermore, a prospective study assessing surgical specimens obtained after neoadjuvant treatment

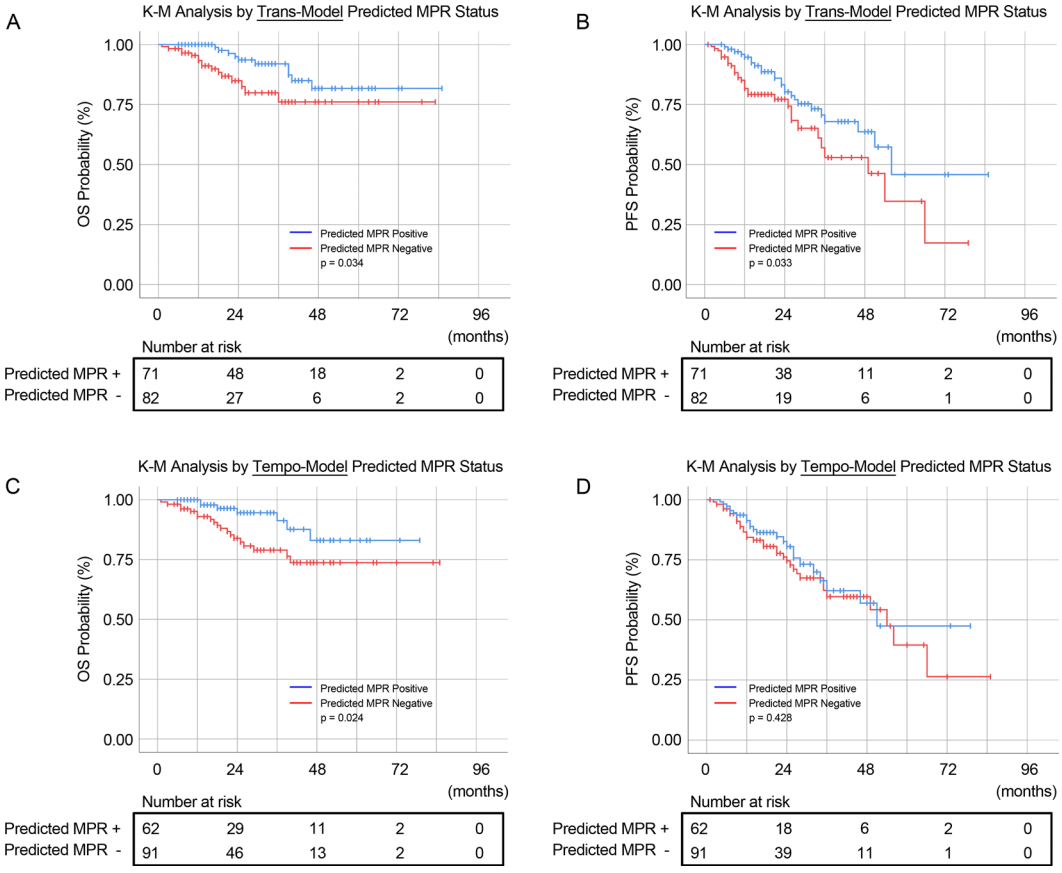

Figure 5 Kaplan-Meier survival analysis in the test cohort. (A) Trans-Model stratified patients into MPR-positive and negative groups with 3-year OS of 87.3% versus 76.1% (p=0.034). (B) Corresponding 5-year PFS rates were 45.8% versus 34.7% (p=0.033). (C) Tempo-Model predicted 3-year OS of 87.6% versus 76.4% (p=0.024). (D) 5-year PFS rates showed no significant difference: 47.5% versus 39.5% (p=0.428). K-M, Kaplan-Meier; MPR, major pathological response; OS, overall survival; PFS, progression-free survival.

demonstrated high diagnostic consistency in interobserver and intraobserver evaluations of the percentage of residual tumor cells, achieving an R^2 value of 0.994.[30] In light of these findings, MPR was selected as the primary predictive indicator for this study.

This study presents a transformer-based framework for predicting the MPR in patients with locally advanced NSCLC undergoing neoadjuvant immunochemotherapy. The primary innovation of this approach lies in the integration of multimodal and multi-temporal data, including radiomics features extracted from multi-sequence longitudinal CT images, pathomics features derived from whole-slide pathology images, and temporal dynamics before and after treatment. Although our framework employs a transformer-based attention mechanism to facilitate feature fusion, its methodological contribution emphasizes the synergistic integration of diverse data sources rather than the fusion method itself. The transformer-based fusion approach uses self-attention and cross-attention mechanisms to effectively capture long-range dependencies and interactions between modalities, serving as a practical tool for data integration. High-resolution CT images enhanced by a GAN and pathomics-derived features were incorporated into the model. The outcomes were subsequently generated using a previously developed integration method based on transformer models.[31] In the test cohort, both the Tempo-Model and Trans-Model exhibited excellent predictive capabilities, with AUC values of 0.852 (95% CI 0.775 to 0.928) and 0.858 (95% CI 0.783 to 0.933), respectively. Based on findings related to 3-year OS and 5-year PFS, the study concluded that the Trans-Model, which integrates pathomics information, demonstrates superior predictive capacity for stratifying patient prognosis compared with the Tempo-Model.

Several predictive biomarkers have been explored to identify populations that can truly benefit from immunotherapy while minimizing the risk of unnecessary immune-related adverse events. These biomarkers include molecular, histological, radiological, and physiological indicators.[32] Some studies have integrated pre-neoadjuvant treatment CT images to develop predictive models.[8 19 21 26 33] However, the models in these studies did not account for the changes in CT images before and after treatment, resulting in AUC values in external validation cohorts ranging from 0.72 to 0.78. Studies that accounted for changes in CT images before and after treatment[8 34 35] reported AUC values ranging from 0.81 to 0.85. However, many of these investigations used conventional fusion techniques, such as feature-level fusion or

feature difference calculations, which may result in the loss of temporal information and consequently limit the overall efficacy of the models. While previous research involved multi-temporal CT imaging, most focused on single-sequence data, with limited studies addressing multi-sequence CT images. Notably, a fusion model was developed by Ye *et al* that incorporated multi-sequence images from both enhanced and plain chest CT scans in the lung window to predict pCR.[20] The model achieved an AUC of 0.866, demonstrating strong predictive efficacy. However, the model was based on a single baseline CT dataset, and further analysis of the model's performance was not conducted. Consequently, it remains unclear whether the use of single-time point data may limit the model's overall efficacy.

Moreover, in a study on breast cancer, Zhang *et al* incorporated imaging data and pathological biopsy specimens to establish a model for predicting pCR, achieving an AUC of 0.933 in the validation cohort.[36] However, it is unfortunate that this was solely a single-center study, lacking an external cohort for validation of the model's efficacy. In a multiomics study on rectal cancer, Feng *et al* included baseline multi-sequence MRI and histopathological data from biopsy specimens, designing a prospective external validation cohort. In this external validation cohort, the model achieved an AUC of 0.812. This indicates that multiomics models can demonstrate good predictive performance; however, there has been no research addressing their application in predicting immune chemotherapy for NSCLC. Furthermore, existing multiomics models have yet to incorporate temporal information into their studies.[37]

In response to the aforementioned circumstances, this study proposes innovative improvements in the areas of image enhancement and multiomics fusion. Our method enables multidimensional characterization of tumors before and after neoadjuvant immunochemotherapy for NSCLC. During the image preprocessing stage, we employed a GANs-based image enhancement technique to increase the resolution of CT images fourfold. Furthermore, an attention mechanism-based transformer fusion approach was used to effectively integrate changes in high-resolution images and multi-sequence information before and after neoadjuvant immunochemotherapy into the model, resulting in the tempo model, which achieved an AUC of 0.852. Finally, by leveraging the aforementioned fusion techniques, we combined radiomic, DL, and histopathological features to construct the Trans-Model, which demonstrated an improved AUC of 0.858, indicating robust model performance. However, further research with larger sample sizes is necessary to analyze and validate how pathomics enhances the prognostic stratification of the Trans-Model concerning PFS. Additionally, it remains to be explored whether this improvement in prognostic stratification will also be reflected in OS with extended follow-up data. The comparatively lower discriminative performance of the Patho-Model may be attributed to limitations in sample size, potential tumor region sampling bias, or inter-institutional staining variability despite rigorous color normalization. Future studies should prioritize expanded multicenter cohorts and standardized automated pathological analysis pipelines to mitigate these confounding factors and enhance feature reproducibility.

This study presents several limitations that warrant consideration. First, despite being a multicenter investigation, the patient enrollment from each center is relatively limited, which may compromise the external validity of the results. Additionally, as a retrospective study, it is inherently prone to selection bias. The restricted sample size further complicates the ability to balance baseline differences between cohorts using methods such as propensity score matching. Second, the follow-up duration for the patients included in this study is limited, precluding the determination of long-term prognostic outcomes. While the observed MPR 3-year survival correlations support short-term predictive utility, extended follow-up is warranted to validate the model's long-term prognostic capability. Moreover, the analysis did not incorporate biomarkers such as PD-L1, as this data was largely unavailable in the samples studied. Third, the manual segmentation of the regions of interest (ROI) was employed, a method that is historically associated with numerous challenges, including significant time consumption, high subjectivity, and poor reproducibility. Lastly, the substantial computational resources required for histopathological research, along with the lengthy processing times, diminish the broad applicability and clinical potential of this methodology. Furthermore, although the model developed in this study demonstrates commendable predictive performance, the use of transformer-based feature fusion techniques has resulted in a reduction in the interpretability of the final output model.

CONCLUSION

In conclusion, the Trans-Model developed in this study effectively integrates multi-temporal, multi-sequence, and multiomics features, demonstrating significant predictive efficacy. It has been shown to outperform existing radiomics, DL, and pathology models in predicting MPR to neoadjuvant immunotherapy in patients with NSCLC. This model assists clinicians in identifying candidates likely to benefit from neoadjuvant immunotherapy, thereby preventing overtreatment, minimizing treatment-related side effects, and advancing personalized cancer therapy.

Author affiliations
[1]Department of Thoracic Surgery, The Fifth Affiliated Hospital of Sun Yat-sen University, Zhuhai, Guangdong, China
[2]Department of Pathology, The Fifth Affiliated Hospital of Sun Yat-sen University, Zhuhai, Guangdong, China
[3]Department of Thoracic Surgery, Guangdong Provincial Key Laboratory of Malignant Tumor Epigenetics and Gene Regulation, Sun Yat-sen Memorial Hospital, Guangzhou, Guangdong, China

[4]Department of Thoracic Surgery, Shenshan Medical Center, Sun Yat-sen Memorial Hospital, Shanwei, Guangdong, China
[5]Department of Cardiothoracic Surgery, Zhongshan City People's Hospital, Zhongshan, Guangdong, China
[6]Department of Radiology, Sun Yat-sen Memorial Hospital, Guangzhou, Guangdong, China

Acknowledgements The authors would like to extend our gratitude to the OneKey platform (https://github.com/OnekeyAI-Platform) for its invaluable contribution to this study.

Contributors Conception and design: XG, BC and QC. Administrative support: QC and BC. Provision of study materials or patients: JH, WZ and XG. Collection and assembly of data: JH, SL, XD, WL and LL. Data analysis and interpretation: XG, WZ and SL. Manuscript writing: All authors. Final approval of manuscript: All authors. The guarantor is BC.

Funding Non-communicable Chronic Diseases-National Science and Technology Major Project (2024ZD0529300).

Competing interests None declared.

Patient consent for publication Not applicable.

Ethics approval The Ethics Committee of Sun Yat-sen Memorial Hospital, as the central board of this study, approved this research (No. SYSKY-2025-217-01). This retrospective study was approved by the Ethics Committee of Sun Yat-sen Memorial Hospital, as the central board of this multicenter study, and informed consent was waived as it involved only the analysis of anonymized data.

Provenance and peer review Not commissioned; externally peer reviewed.

Data availability statement Data are available upon reasonable request.

ORCID iD
Baishen Chen https://orcid.org/0009-0001-2164-7036

REFERENCES

1 Siegel RL, Giaquinto AN, Jemal A. Cancer statistics, 2024. *CA Cancer J Clin* 2024;74:12–49.
2 Lahiri A, Maji A, Potdar PD, *et al*. Lung cancer immunotherapy: progress, pitfalls, and promises. *Mol Cancer* 2023;22:40.
3 Heymach JV, Harpole D, Mitsudomi T, *et al*. Abstract CT005: AEGEAN: A phase 3 trial of neoadjuvant durvalumab + chemotherapy followed by adjuvant durvalumab in patients with resectable NSCLC. *Cancer Res* 2023;83:CT005.
4 Cascone T, Awad MM, Spicer JD, *et al*. LBA1 CheckMate 77T: Phase III study comparing neoadjuvant nivolumab (NIVO) plus chemotherapy (chemo) vs neoadjuvant placebo plus chemo followed by surgery and adjuvant NIVO or placebo for previously untreated, resectable stage II–IIIb NSCLC. *Ann Oncol* 2023;34:S1295.
5 Forde PM, Spicer J, Lu S, *et al*. Neoadjuvant Nivolumab plus Chemotherapy in Resectable Lung Cancer. *N Engl J Med* 2022;386:1973–85.
6 Yue D, Tan L, Xu S, *et al*. 108O Surgical outcomes from RATIONALE-315: Randomized, double-blind, phase III study of perioperative tislelizumab with neoadjuvant chemotherapy in resectable NSCLC. *ESMO Open* 2024;9:102687.
7 Zhao J, Hao S, Li Y, *et al*. Comparative Efficacy and Safety of Neoadjuvant Immunotherapy with Chemotherapy versus Chemotherapy Alone in Non-Small Cell Lung Cancer: A Propensity Score and Inverse Probability Treatment Weighting Analysis. *Immunotargets Ther* 2023;12:113–33.
8 Yang N, Yue H-L, Zhang B-H, *et al*. Predicting pathological response to neoadjuvant or conversion chemoimmunotherapy in stage IB-III non-small cell lung cancer patients using radiomic features. *Thorac Cancer* 2023;14:2869–76.
9 Wang C, Chen K-N, Chen Q, *et al*. Neoadjuvant nivolumab plus chemotherapy versus chemotherapy for resectable NSCLC: subpopulation analysis of Chinese patients in CheckMate 816. *ESMO Open* 2023;8:102040.
10 Wakelee H, Liberman M, Kato T, *et al*. Perioperative Pembrolizumab for Early-Stage Non-Small-Cell Lung Cancer. *N Engl J Med* 2023;389:491–503.
11 Felip E, Altorki N, Zhou C, *et al*. Adjuvant atezolizumab after adjuvant chemotherapy in resected stage IB-IIIA non-small-cell lung cancer (IMpower010): a randomised, multicentre, open-label, phase 3 trial. *Lancet* 2021;398:1344–57.
12 Takada K, Takamori S, Brunetti L, *et al*. Impact of Neoadjuvant Immune Checkpoint Inhibitors on Surgery and Perioperative Complications in Patients With Non-small-cell Lung Cancer: A Systematic Review. *Clin Lung Cancer* 2023;24:581–90.
13 Cascone T, William WN Jr, Weissferdt A, *et al*. Neoadjuvant nivolumab or nivolumab plus ipilimumab in operable non-small cell lung cancer: the phase 2 randomized NEOSTAR trial. *Nat Med* 2021;27:504–14.
14 Gao S, Li N, Gao S, *et al*. Neoadjuvant PD-1 inhibitor (Sintilimab) in NSCLC. *J Thorac Oncol* 2020;15:816–26.
15 Forde PM, Spicer J, Girard N, *et al*. 84O Neoadjuvant nivolumab (N) + platinum-doublet chemotherapy (C) for resectable NSCLC: 3-y update from CheckMate 816. *J Thorac Oncol* 2023;18:S89–90.
16 Wakelee HA, Liberman M, Kato T, *et al*. KEYNOTE-671: Randomized, double-blind, phase 3 study of pembrolizumab or placebo plus platinum-based chemotherapy followed by resection and pembrolizumab or placebo for early stage NSCLC. *JCO* 2023;41:LBA100.
17 Lu S, Wu L, Zhang W, *et al*. Perioperative toripalimab + platinum-doublet chemotherapy vs chemotherapy in resectable stage II/III non-small cell lung cancer (NSCLC): Interim event-free survival (EFS) analysis of the phase III Neotorch study. *JCO* 2023;41:425126.
18 Provencio M, Nadal E, Insa A, *et al*. Neoadjuvant chemotherapy and nivolumab in resectable non-small-cell lung cancer (NADIM): an open-label, multicentre, single-arm, phase 2 trial. *Lancet Oncol* 2020;21:1413–22.
19 She Y, He B, Wang F, *et al*. Deep learning for predicting major pathological response to neoadjuvant chemoimmunotherapy in non-small cell lung cancer: A multicentre study. *EBioMedicine* 2022;86:104364.
20 Ye G, Wu G, Qi Y, *et al*. Non-invasive multimodal CT deep learning biomarker to predict pathological complete response of non-small cell lung cancer following neoadjuvant immunochemotherapy: a multicenter study. *J Immunother Cancer* 2024;12:e009348.
21 Ye G, Wu G, Zhang C, *et al*. CT-based quantification of intratumoral heterogeneity for predicting pathologic complete response to neoadjuvant immunochemotherapy in non-small cell lung cancer. *Front Immunol* 2024;15:1414954.
22 Vaswani A, Shazeer N, Parmar N, *et al*. Attention Is All You Need. *arXiv* 2017.
23 International Conference on Learning Representations. An image is worth 16x16 words: transformers for image recognition at scale. 2021.
24 Liang Z, Zhao K, Liang G, *et al*. MAXFormer: Enhanced transformer for medical image segmentation with multi-attention and multi-scale features fusion. *Knowl Based Syst* 2023;280:110987.
25 Hellmann MD, Chaft JE, William WN Jr, *et al*. Pathological response after neoadjuvant chemotherapy in resectable non-small-cell lung cancers: proposal for the use of major pathological response as a surrogate endpoint. *Lancet Oncol* 2014;15:e42–50.
26 Qu W, Chen C, Cai C, *et al*. Non-invasive prediction for pathologic complete response to neoadjuvant chemoimmunotherapy in lung cancer using CT-based deep learning: a multicenter study. *Front Immunol* 2024;15:1327779.
27 Yue D, Wang W, Liu H, *et al*. LBA58 Pathological response to neoadjuvant tislelizumab (TIS) plus platinum-doublet (PtDb) chemotherapy (CT) in resectable stage II-IIIA NSCLC patients (pts) in the phase III (Ph3) RATIONALE-315 trial. *Ann Oncol* 2023;34:S1299.
28 Provencio M, Nadal E, González-Larriba JL, *et al*. Perioperative Nivolumab and Chemotherapy in Stage III Non–Small-Cell Lung Cancer. *N Engl J Med* 2023;389:504–13.
29 Heymach JV, Harpole D, Mitsudomi T, *et al*. Perioperative Durvalumab for Resectable Non-Small-Cell Lung Cancer. *N Engl J Med* 2023;389:1672–84.

30 Weissferdt A, Pataer A, Vaporciyan AA, *et al*. Agreement on Major Pathological Response in NSCLC Patients Receiving Neoadjuvant Chemotherapy. *Clin Lung Cancer* 2020;21:341–8.
31 Zhang W, Gan X, Chen W, *et al*. Attention mechanism-based habitat analysis for predicting pleural invasion and prognosis of pulmonary nodules. *Transl Lung Cancer Res* 2025;14:1596–610.
32 Lotze MT, Cottrell T, Bifulco C, *et al*. SITC Clinical Immuno-Oncology Network (SCION) commentary on measurement and interpretation of essential biomarkers in early clinical trials. *J Immunother Cancer* 2024;12:e008655.
33 Huang D, Lin C, Jiang Y, *et al*. Radiomics model based on intratumoral and peritumoral features for predicting major pathological response in non-small cell lung cancer receiving neoadjuvant immunochemotherapy. *Front Oncol* 2024;14:1348678.
34 Lin Q, Wu HJ, Song QS, *et al*. CT-based radiomics in predicting pathological response in non-small cell lung cancer patients receiving neoadjuvant immunotherapy. *Front Oncol* 2022;12:937277.
35 Han X, Wang M, Zheng Y, *et al*. Delta-radiomics features for predicting the major pathological response to neoadjuvant chemoimmunotherapy in non-small cell lung cancer. *Eur Radiol* 2024;34:2716–26.
36 Zhang J, Wu Q, Yin W, *et al*. Development and validation of a radiopathomic model for predicting pathologic complete response to neoadjuvant chemotherapy in breast cancer patients. *BMC Cancer* 2023;23:431.
37 Feng L, Liu Z, Li C, *et al*. Development and validation of a radiopathomics model to predict pathological complete response to neoadjuvant chemoradiotherapy in locally advanced rectal cancer: a multicentre observational study. *Lancet Digit Health* 2022;4:e8–17.